Electronic Supplementary Material (ESI) for Soft Matter.

Supplementary information: Scalloped pattern deposition during spreading and drying polymer droplets

Ahmed M. Othman[1], Andreas. S. Poulos[2], Ophelie Torres[2], and Alexander. F. Routh[1]

[1]Department of Chemical Engineering and Biotechnology, University of Cambridge, Philippa Fawcett Dr, Cambridge, CB3 0AS, United Kingdom

[2]Unilever R&D Port Sunlight, Quarry Road East, Wirral, CH63 3JW, United Kingdom

Contents

Viscosity and Shear Rate Behaviour of PVP in Ehanol Solution

Fig. S–1 presents the viscosity of a polymer solution composed of polyvinylpyrrolidone (PVP) in ethanol. The measurements were conducted using a Kinexus Pro+ rheometer with a cup and bob accessory. Notably, the results reveal a constant viscosity across the range of shear rates investigated. Within the selected range of shear rates, shear thinning does not appear to occur, likely because the shear rate is insufficient.

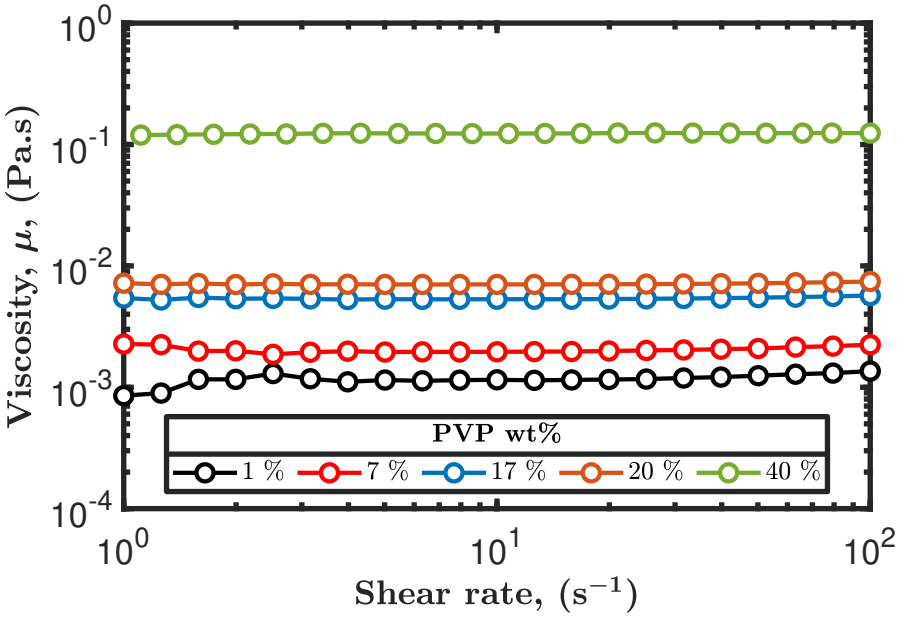

Fig. S–1: Viscosity as a function of shear rate for different concentrations of 10 kDa PVP in ethanol solutions measured at 22°C.

Formation of Uniform Thin Film

The spreading process of a 1 wt% PVP in ethanol droplet on a glass slide gives rise to the emergence of a uniform, thin film during the initial stages of Marangoni flow, as shown in Fig. S–2. This thin film exhibits a consistent thickness throughout. It is noteworthy that the thin film is sustained by the main droplet, serving as a fluid reservoir. Findings from a prior investigation on Marangoni flow-induced ethanol and water films on inclined surfaces have reported analogous observations.[5,18]

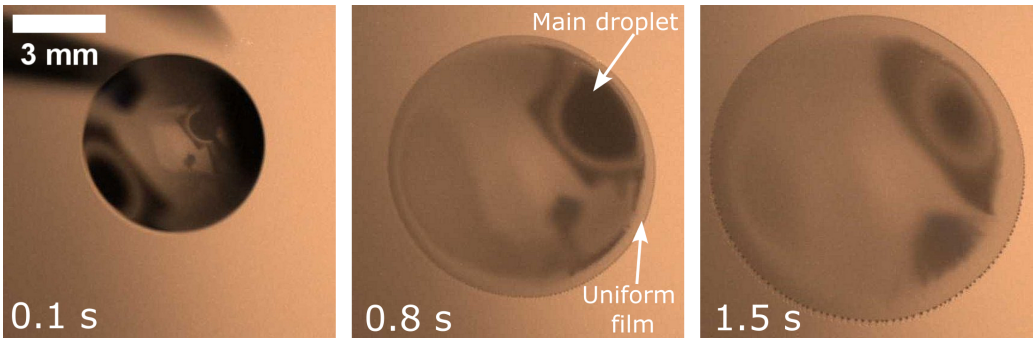

Fig. S–2: Top-view images taken for a 1 wt% PVP in ethanol droplet deposited on a glass slide at 22°C showing the uniform film extended from the main droplet.

Influence of Surface Wettability on the Instability

Fig. S–3 displays the deposition of PVP in ethanol droplets with varying concentrations on a polytetrafluoroethylene (PTFE) substrate, captured 60 seconds after deposition. Fig.S–4 presents a side-view image of a 5 wt% PVP in ethanol droplet on a PTFE substrate, demonstrating the formation of a finite contact angle. Furthermore, Fig. S–3 and Fig. S–4 demonstrate the stable nature of the contact line, characterised by the absence of the scalloped pattern.

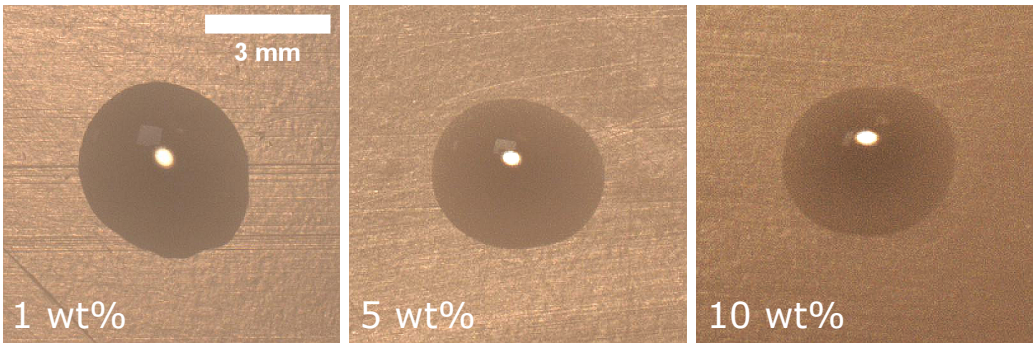

Fig. S–3: Top-view images of PVP in ethanol drops with different initial concentrations after 60 seconds from deposition on a hydrophobic polytetrafluoroethylene (PFTE) at 22°C.

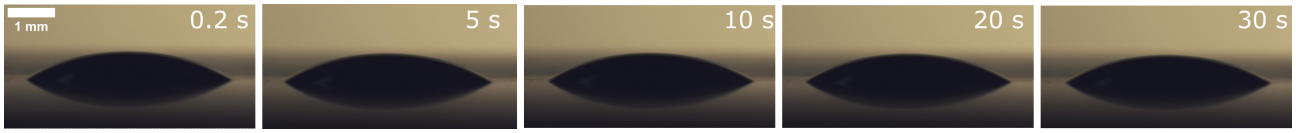

Fig. S–4: Side-view image of a 5 wt% PVP in ethanol droplet deposited on a PTFE substrate captured at different time intervals.

Influence of Solvent Evaporation on the Instability

Fig. S–5 presents top-view images depicting the film morphology of PVP in ethanol droplets with various initial polymer concentrations. These images were captured in an environment saturated with ethanol vapour. Despite the substantial reduction or suppression of evaporation, the observed instability persists at the droplet edge. Furthermore, Table S–1 provides a comparison of the instability wavelength values resulting from droplet spreading in an ethanol-saturated environment and under atmospheric conditions.

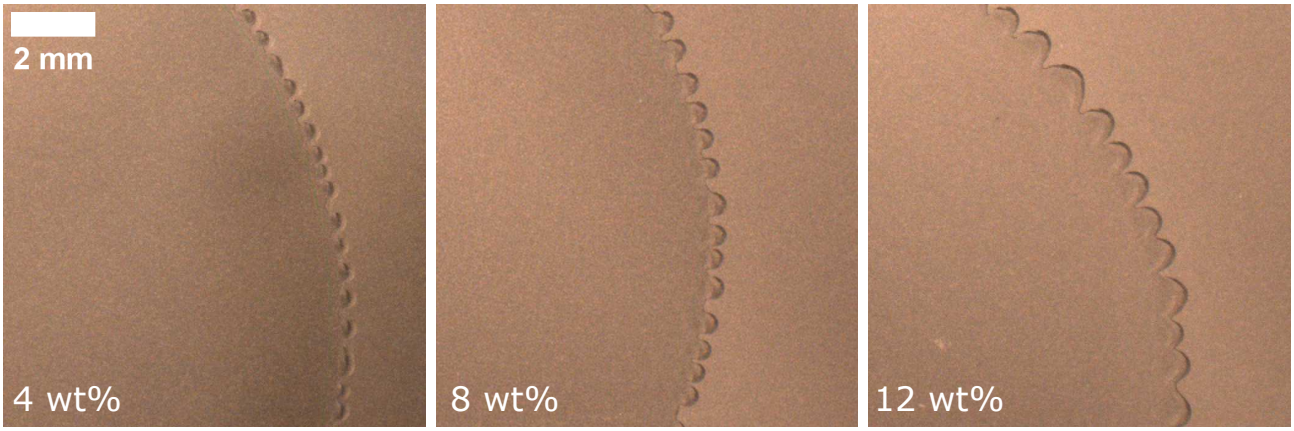

Fig. S–5: Top-view images of different PVP in ethanol droplets at 22°C in an ethanol-saturated conditions to reduce ethanol evaporation from the droplet.

Table S–1: Comparison between instability wavelengths in an ethanol-saturated environment and under atmospheric environment for different PVP in ethanol droplets deposited on a glass slide

PVP concentration (wt%)	Wavelength in an ethanol-saturated environment (mm)	Wavelength in atmospheric conditions (mm)
4	0.49 ± 0.09	0.43 ± 0.06
8	0.79 ± 0.16	0.78 ± 0.15
12	1.08 ± 0.21	1.25 ± 0.28

Mathematical Formulation

Consider a thin droplet containing a dissolved polymer in a single solvent deposited on a solid flat substrate, as depicted in Fig. S–6a. The fluid density is ρ_0, viscosity μ_0, initial droplet height is h_0^* and radius is R_0^*. For simplicity, a Cartesian coordinate system is used to derive the relevant equations, where the horizontal coordinate is x, the vertical coordinate is z and the transverse coordinate is y. The flow of the droplet is governed by the Navier Stokes equations.

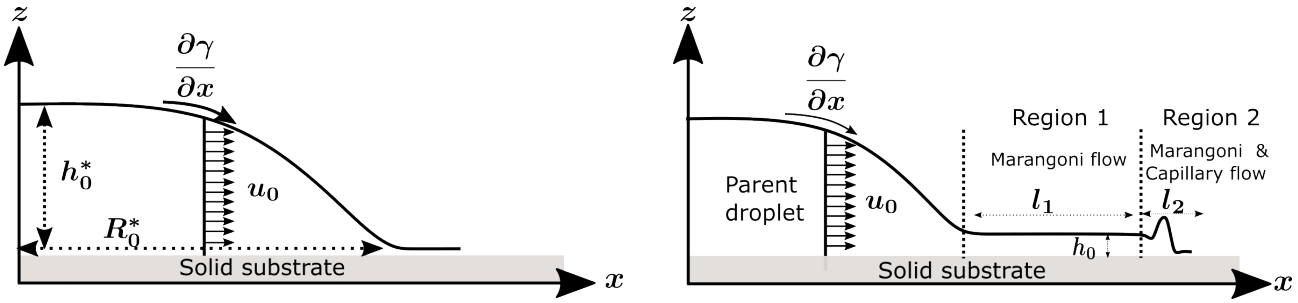

(a) (b)

Fig. S–6: (a) A sketch that shows a droplet on a flat solid substrate with a no-slip boundary and (b) A sketch showing the associated length scales as a result of droplet spreading due to solutal Marangoni on a flat solid substrate.

Scaling and Assumptions

The horizontal coordinates are scaled by the radius R_0^* and the vertical distances by the height of the droplet h_0^*. The aspect ratio of a thin droplet is $\epsilon = h_0^*/R_0^* < 1$. The horizontal velocities are scaled arbitrarily by u_0 and the vertical velocity is scaled by $w^* = \epsilon u_0$. Upon scaling, the Reynolds number, ($Re = \rho_0 u_0 h_0^*/\mu_0$), is found to be small, and the lubrication approximation assumption holds as ϵRe and $\epsilon^2 \ll 1$. Applying the lubrication approximation to the non-dimensionalised Navier Stokes and continuity equations yields

$$\frac{1}{\mu}\frac{\partial P}{\partial x} = \frac{\partial^2 u}{\partial z^2}, \text{ and } \frac{1}{\mu}\frac{\partial P}{\partial y} = \frac{\partial^2 v}{\partial z^2}. \tag{1}$$

The boundary condition at the solid-liquid interface is non-slip, i.e., at $z = 0$, $u = 0$ and $v = 0$. The tangential shear stress at the air-liquid interface is taken as a constant shear due to the

solutal surface tension gradient, which only acts horizontally

$$z = h, \qquad \mu \frac{\partial u}{\partial z} = \frac{\partial \gamma}{\partial x}. \tag{2}$$

The horizontal velocities are determined by integrating equation 1. The height-averaged velocities denoted as $\hat{u}$ and $\hat{v}$, are determined by

$$\hat{u} = \frac{1}{h}\int_0^h u\, dz = -\frac{h^2}{3\mu}\frac{\partial P}{\partial x} + \frac{1}{2\mu}\frac{\partial \gamma}{\partial x}h, \text{ and } \hat{v} = \frac{1}{h}\int_0^h v\, dz = -\frac{h^2}{3\mu}\frac{\partial P}{\partial y}. \tag{3}$$

The pressure P is determined by the Young-Laplace equation $P = -\gamma\kappa$, where γ is the surface tension and κ is the mean curvature.[6,7,14] Within the lubrication approximation, the mean curvature can be found using differential geometry $\kappa = \nabla^2 h$.[7] The pressure term is

$$P = -\gamma\nabla^2 h = -\gamma\left(\frac{\partial^2 h}{\partial x^2} + \frac{\partial^2 h}{\partial y^2}\right). \tag{4}$$

Substituting the pressure term into equation 3, the height averaged velocities are given by

$$\hat{u} = \frac{h^2}{3\mu}\frac{\partial}{\partial x}(\gamma\nabla^2 h) + \frac{1}{2\mu}\frac{\partial \gamma}{\partial x}h, \text{ and } \hat{v} = \frac{h^2}{3\mu}\frac{\partial}{\partial y}(\gamma\nabla^2 h). \tag{5}$$

Equation 5 describes the two contributions of the horizontal velocity. The first describes the velocity due to curvature and the second contribution is the solutal Marangoni shear stress. The governing equation of the film thickness h can be found using a simple mass balance to get a time-dependent partial differential equation[8,13,15]

$$\frac{\partial h}{\partial t} = -\frac{\partial}{\partial x}(h\hat{u}) - \frac{\partial}{\partial y}(h\hat{v}). \tag{6}$$

Second Spreading Dynamic

During this regime, the main droplet acts as a fluid reservoir for the extended thin film and replenishes the fluid. Therefore, it is reasonable to assume the extended film from the droplet has a uniform thickness, i.e., evaporation is negligible in this region. Two length scales have been identified experimentally. The first is the uniform thin film away from the triple contact line. The second is near the triple contact line. Various spreading problems were modelled similarly, where different forces influence different length scales,[9,11,16] which are represented in Fig. S–6b.

A new scaling will be used for both length scales, as different forces influence each region. In the region near the droplet meniscus, i.e., region 1, the following scalings are introduced $\bar{x} = \dfrac{x}{l_1},\ \bar{y} = \dfrac{y}{l_1},\quad \bar{z} = \dfrac{z}{h_0},\quad \bar{h} = \dfrac{h}{h_0},\ \bar{u} = \dfrac{\hat{u}}{u_0}.$

The quantities with overbars are the dimensionless variables. The lubrication approximation still holds as the thickness of the extended film is small $h_0 \ll h_0^*$. Introducing the scalings to equation 5 provides

$$\bar{u} = \left(\frac{h_0^3\gamma}{3\mu l_1^3 u_0}\right)\bar{h}^2\frac{\partial}{\partial\bar{x}}(\bar{\nabla}^2\bar{h}) + \left(\frac{h_0}{2\mu u_0}\frac{\partial\gamma}{\partial x}\right)\bar{h}. \tag{7}$$

In this region, the curvature term is neglected as $(\epsilon^3\gamma/3\mu u_0) \ll 1$. The curvature is only significant at the edge of the thin film. Hence, the flow is driven mainly by a surface tension gradient, i.e., the solutal Marangoni flow. The velocity scale u_0 will be used to match the solution to the region near the triple contact line and is given as

$$u_0 = \left(\frac{h_0}{2\mu}\frac{\partial\gamma}{\partial x}\right). \tag{8}$$

The region near the triple contact line is of interest, as this is where the instability occurs. The curvature term is important as this is where the ridge is occurring, which sets a different length scale. The scaling in this region is as follows

$\bar{x} = \dfrac{x}{l_2},\ \bar{y} = \dfrac{y}{l_2},\quad \bar{z} = \dfrac{z}{h_0},\quad \bar{h} = \dfrac{h}{h_0},\ \bar{u} = \dfrac{\hat{u}}{u_0}.$

The length scale of this region is denoted as l_2 and can be derived from equation 7 as

$$l_2 = h_0 \left(\frac{\gamma}{3\mu u_0} \right)^{1/3}. \tag{9}$$

Subsequently, the non-dimensional velocities near region 2 are given by

$$\bar{u} = \bar{h}^2 \frac{\partial}{\partial \bar{x}} (\bar{\nabla}^2 \bar{h}) + \bar{h}, \text{ and } \bar{v} = \bar{h}^2 \frac{\partial}{\partial \bar{y}} (\bar{\nabla}^2 \bar{h}). \tag{10}$$

Substituting the resulting velocities into equation 6 yields the governing equation of region 2 near the contact line

$$\frac{\partial \bar{h}}{\partial \bar{t}} = -\frac{\partial}{\partial \bar{x}} \left(\bar{h}^3 \frac{\partial}{\partial \bar{x}} (\bar{\nabla}^2 \bar{h}) + \bar{h^2} \right) - \frac{\partial}{\partial \bar{y}} \left(\bar{h}^3 \frac{\partial}{\partial \bar{y}} (\bar{\nabla}^2 \bar{h}) \right). \tag{11}$$

The base solution for equation 11 is assumed to be independent of the y-coordinate, indicating that flow in the transverse direction will not develop any structure. Hence, equation 11 can be reduced to

$$\frac{\partial \bar{h}}{\partial \bar{t}} = -\frac{\partial}{\partial \bar{x}} \left(\bar{h}^3 \frac{\partial}{\partial \bar{x}} (\bar{\nabla}^2 \bar{h}) + \bar{h^2} \right). \tag{12}$$

The absence of the evaporation term in equation 12 can be attributed to the underlying assumption that it does not exert any discernible influence on the thickness of the uniform film. This assumption is based on our experimental observations, where it has been noted that the parent droplet compensates for any fluid loss experienced by the thin film (in region 1, as depicted in Fig S–6b), thereby sustaining its uniform thickness. This observation has been reported previously in binary mixtures evaporating on a tilted substrate.[5,18]

Surface Tension Gradient and Marangoni Flow Velocity

At the air-liquid interface, the magnitude of the shear stress due to concentration gradients can be quantified using the solvent concentration. The dimensional mass balance is given by[7,19]

$$\frac{\partial}{\partial t}(Ch) = -\frac{\partial}{\partial x}(hCu) - E, \tag{13}$$

where C is the concentration of the volatile liquid component and E is the evaporation rate. Within the lubriacation approximation, it is assumed that there is no vertical variation in concentration, i.e. $\dfrac{\partial C}{\partial z} = 0$. It is also assumed that the evaporation rate is uniform across the droplet, based on the premise that there exists an external velocity field to mix any external air.[15] This assumption of a constant evaporation rate is applied to the entire droplet. Hence, using equation 6, the concentration of the solvent is given by

$$h\frac{\partial C}{\partial t} = -hu\frac{\partial C}{\partial x} - E. \tag{14}$$

Assuming the variation of concentration in the extended film with time is negligible as the parent drop continuously replenishes the film, the change in volatile liquid concentration as a function of distance is given by

$$\frac{\partial C}{\partial x} = -\frac{E}{hu}. \tag{15}$$

The shear stress at the air-liquid interface can be written as

$$\frac{\partial \gamma}{\partial x} = \frac{\partial \gamma}{\partial C}\frac{\partial C}{\partial x}. \tag{16}$$

For the surface tension in the binary mixture, as a function of the volatile liquid composition, a linear dependence was assumed

$$\frac{\partial \gamma}{\partial C} = \frac{\nabla \gamma}{\nabla C} = \frac{\gamma_A - \gamma_B}{C_A - C_B}, \tag{17}$$

where subscript A refers to ethanol and B to the polymer containing trace water. Using equations 15 and 17, the shear stress can be obtained as

$$\frac{\partial \gamma}{\partial x} = \frac{E(\gamma_B - \gamma_A)}{hu(C_A - C_B)}. \tag{18}$$

The magnitude of the solutal Marangoni velocity in equation 8 is given by

$$u_0 = \left(\frac{E(\gamma_B - \gamma_A)}{2\mu(C_A - C_B)} \right)^{1/2}. \tag{19}$$

Equation 19 represents a constant velocity in the extended thin film resulting from solutal Marangoni shear flow. This velocity will be used to determine the length scale of region 2.

Boundary and Initial Conditions

Four boundary conditions are needed in order to obtain a solution to equation 12. The length of the computational domain size is defined as L_x. The following boundary conditions are selected

$$\bar{h}(0,\bar{t}) = 1 \quad \bar{h}(L_x,\bar{t}) = b, \text{ and } \frac{\partial \bar{h}}{\partial \bar{x}}(0,\bar{t}) = \frac{\partial \bar{h}}{\partial \bar{x}}(L_{\bar{x}},\bar{t}) = 0. \tag{20}$$

Away from the edge and towards region 1, the film height is set to unity. Numerical solutions for a moving contact line lead to a singularity, which occurs as a result of the assumption of the no-slip boundary condition at $z = 0$.[2] As the contact line advances, a multivalued velocity field at the triple contact line is produced as the liquid replaces air. One approach to treating the contact line singularity is to assume the solid surface is pre-wetted by a thin layer of fluid, known as a precursor film.[11,12,20] Therefore, as $\bar{x} \to L_{\bar{x}}$, the boundary condition was selected to be equal to a precursor film that is consistent with complete wetting.[4]

A hyperbolic tangent function is used to approximate the initial profile of the thin film h_0. This

function is a smooth curve that connects two different flat regions and is given by[11]

$$h_0 = \frac{(1+b)}{2} - \frac{(1-b)}{2}\tanh(x - x_f), \tag{21}$$

where x_f is the contact line position in the domain $L_{\bar{x}}$. The choice of this initial boundary condition is arbitrary.

Numerical Results

A second-order finite difference scheme is used, following the method illustrated in Kondic[11]. The governing equation is therefore linearised using this approximation. A Matlab implicit solver was used to solve the resulting equations. Fig. S–7a shows an important feature of thin film spreading with a dynamic contact line, which is the occurrence of a capillary ridge close to the contact line. Fig. S–7b shows the effect of different precursor film thicknesses on the front ridge. It is noticed that by reducing the precursor thickness, the ridge appears to be more pronounced than with a larger precursor thickness value.

Travelling Wave Solution

After an initial period, the flow profile develops into a travelling wave with constant speed, as shown in Fig. S–7a. A coordinate transformation is used to define the solution of this travelling wave. A moving frame is selected $\xi = \bar{x} - c\bar{t}$ where c is the wave speed and $H_0(\xi) = \bar{h}(\bar{x}, \bar{t})$ is the film thickness.

The new coordinates are substituted into equation 12 yielding

$$-c\frac{\partial H_0}{\partial \xi} = -\frac{\partial}{\partial \xi}\left[H_0\left(\frac{\partial^3 H_0}{\partial \xi^3}\right) + H_0^2\right]. \tag{22}$$

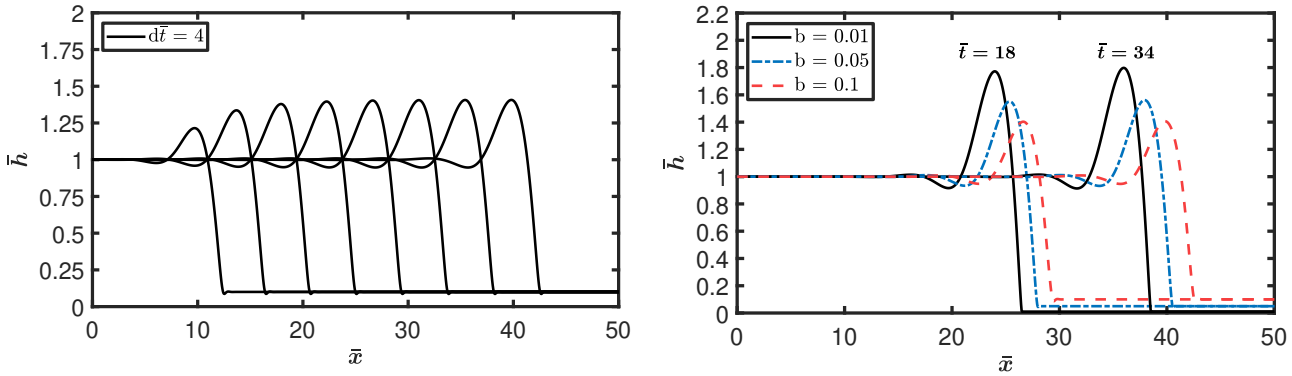

(a) (b)

Fig. S–7: (a) Time evolution of a thin liquid film spreading on a horizontal substrate at different time intervals ($d\bar{t} = 4$) with a precursor thickness $b = 0.1$ and a domain length of $L_x = 50$ and (b) Numerical solution for a thin film spreading profile on a horizontal substrate at different times and different precursor film thicknesses.

Linear Stability Analysis

A linear stability analysis is performed to investigate the stability of PVP in ethanol droplets. As experimentally shown, undulations occur in the film after the initial spreading in the transverse direction. To capture this, a small perturbation is introduced in the y direction to the travelling wave solution, yielding

$$H(\xi, \bar{y}, \bar{t}) = H_0(\xi) + \varsigma H_1(\xi, \bar{y}, \bar{t}), \tag{23}$$

where $H_0(\xi)$ is the base solution obtained from equation 22 and $\varsigma H_1(\xi, y, t)$ is the small perturbation. Substituting equation 23 into the height governing equation 11 and retaining terms of $O(\varsigma)$, linearises the governing equation 11 and gives a fourth-order equation in terms of the perturbation H_1

$$\frac{\partial H_1}{\partial \bar{t}} = -\frac{\partial}{\partial \xi}\left[2H_0H_1 + H_0^3\frac{\partial^3 H_1}{\partial \xi^3} + H_0^3\frac{\partial^3 H_1}{\partial y^2 \partial \xi} + 3H_0^2H_1\frac{\partial^3 H_0}{\partial \xi^3}\right] - \frac{\partial}{\partial y}\left[H_0^3\frac{\partial^3 H_1}{\partial \xi^2 \partial y} + h_0^3\frac{\partial^3 H_1}{\partial y^3}\right] + c\frac{\partial H_1}{\partial \xi}. \tag{24}$$

Equation 24 can be simplified by expressing the perturbation term as $H_1 = H_1(\xi, \bar{t})\exp^{i\kappa\bar{y}}$.[1,11,17] Substituting into equation 24, the evolution of the perturbation can be expressed as

$$\frac{\partial H_1}{\partial \bar{t}} = -\sum_{i=0}^{4} \mathbb{A}_i {H_1}^i, \tag{25}$$

where $\mathbb{A}$ is a linear operator given as

$$\mathbb{A}_0 = \left[\frac{\partial H_0}{2\partial\xi} + 3\frac{\partial H_0^2}{\partial\xi}\frac{\partial^3 H_0}{\partial\xi^3} + 3H_0^2\frac{\partial^4 H_0}{\partial\xi^4} + H_0^3\kappa^4\right],\ \mathbb{A}_1 = \left[2H_0 - \frac{\partial H_0^3}{\partial\xi}\kappa^2 + 3H_0^2\frac{\partial^3 H_0}{\partial\xi^3} - c\right],$$

$$\mathbb{A}_2 = \left[-2H_0^3\kappa^2\right],\ \mathbb{A}_3 = \left[\frac{\partial H_0^3}{\partial\xi}\right],\ \mathbb{A}_4 = \left[H_0^3\right],$$

and κ represents the perturbation wavenumber in the transverse direction. The perturbation far away from the edge of the fluid is decaying; hence, four boundary conditions are used to solve equation 25

$$\begin{aligned} H_1,\ \frac{\partial H_1}{\partial\xi} \to 0 \quad \text{as} \quad \xi \to +\infty, \\ H_1,\ \frac{\partial H_1}{\partial\xi} \to 0 \quad \text{as} \quad \xi \to -\infty. \end{aligned} \tag{26}$$

The perturbation equation can be solved using a second-order finite difference method in a domain between [0, L]. The perturbation solution H_1 is assumed to have an exponential dependence with time and is given by[11]

$$H_1(\xi, \bar{t}) = \phi(\xi)e^{\omega\bar{t}}, \tag{27}$$

where ω is the growth rate of the perturbation. The growth rate ω determines the stability of the contact line. If the value of $\omega > 0$ then the perturbations grow with time; if the value of $\omega < 0$ then the perturbations decay and the contact line is stable.

As it can be seen from Fig. S–8, the system is unstable to disturbances with a wavenumber between $0 < \kappa \leq 0.55$. The influence of the precursor film is small, as the most unstable wavelength ranges from $\kappa = 0.35$ to 0.38 for different values of b. This is similar to the wavenumbers found in a steady-state Marangoni flow that is driven by thermal gradients on a vertical substrate.[3,9,10] The most unstable wavelength that will be compared to the experimental observation corresponds to $\kappa = 0.37$. The dimensionless wavelength can be calculated

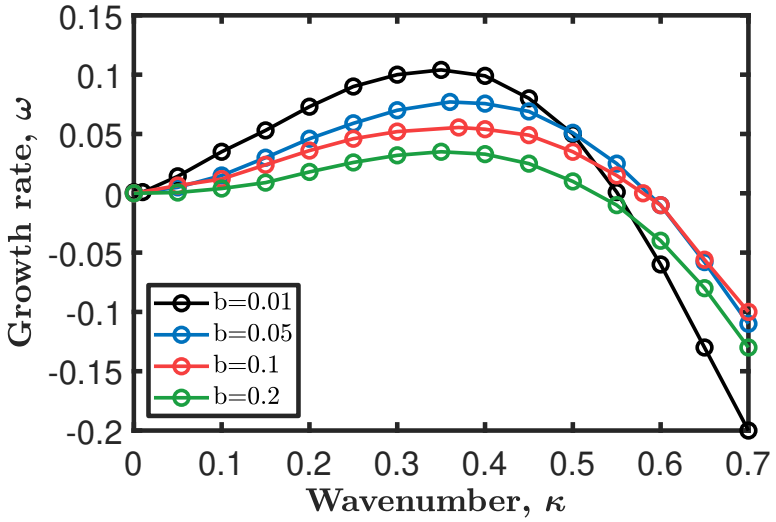

Fig. S–8: The dimensionless growth rate as a function of the wavenumber for different precursor film thicknesses.

according to $\bar{\lambda} = 2\pi/\kappa$. The dimensional wavelength is scaled by the region 2 length scale, hence $\lambda = 17h_0 \left(\frac{\gamma}{3\mu u_0}\right)^{1/3}$.

References

[1] Bertozzi, A. L. and Brenner, M. P. (1998). Linear stability and transient growth in driven contact lines. *Phys. Fluids*, 9(3):530–539.

[2] Bertozzi, A. L., Münch, A., Fanton, X., and Cazabat, A. M. (1998). Contact line stability and "undercompressive shocks" in driven thin film flow. *Phys. Rev. Lett.*, 81(23):5169–5172.

[3] Davis, J. M. and Troian, S. M. (2003). Influence of attractive van der Waals interactions on the optimal excitations in thermocapillary-driven spreading. *Phys. Rev. E*, 67(1):016308.

[4] De Gennes, P. G. (1985). Wetting: statics and dynamics. *Rev. of Modern Phys.*, 57(3):827–863.

[5] de Ryck, A. (1999). Instability of a meniscus due to surface tension gradient-driven flow. *J. Colloid Interface Sci*, 209(1):10–15.

[6] Diez, J. A. and Kondic, L. (2002). Computing three-dimensional thin film flows including contact lines. *J. Comput. Phys.*, 183(1):274–306.

[7] Eales, A. D., Routh, A. F., Dartnell, N., and Simon, G. (2015). Evaporation of pinned droplets containing polymer - an examination of the important groups controlling final shape. *AIChE J.*, 61(5):1759–1767.

[8] Fischer, B. J. (2002). Particle convection in an evaporating colloidal droplet. *Langmuir*, 18(1):60–67.

[9] Kataoka, D. E. and Troian, S. M. (1997). A theoretical study of instabilities at the advancing front of thermally driven coating films. *J. Colloid Interface Sci.*, 192(2):350–362.

[10] Kataoka, D. E. and Troian, S. M. (1999). Patterning liquid flow on the microscopic scale. *Nature*, 402(6763):794–797.

[11] Kondic, L. (2003). Instabilities in gravity driven flow of thin fluid films. *SIAM Rev.*, 45(1):95–115.

[12] Moriarty, J. A., Schwartz, L. W., and Tuck, E. O. (1991). Unsteady spreading of thin liquid films with small surface tension. *Phys. Fluids A*, 3(5):733–742.

[13] Oron, A., Davis, S. H., and Bankoff, S. G. (1997). Long-scale evolution of thin liquid films. *Rev. Mod. Phys.*, 69(3):931–980.

[14] Pahlavan, A. A., Cueto-Felgueroso, L., Hosoi, A. E., McKinley, G. H., and Juanes, R. (2018). Thin films in partial wetting: Stability, dewetting and coarsening. *J. Fluid Mech.*, 845:642–681.

[15] Routh, A. F. (2013). Drying of thin colloidal films. *Rep. Prog. Phys.*, 76(4):046603.

[16] Spaid, M. A. and Homsy, G. M. (1996). Stability of newtonian and viscoelastic dynamic contact lines. *Phys. Fluids*, 8(2):460–478.

[17] Troian, S. M., Joanny, J. F., and Safran, S. A. (1989). Fingering instabilities of driven spreading films. *Europhys. Lett.*, 10(1):25–30.

[18] Vuilleumier, R., Ego, V., Neltner, L., and Cazabat, A. M. (1995). Tears of wine: the stationary state. *Langmuir*, 11(10):4117–4121.

[19] Warner, M. R., Craster, R. V., and Matar, O. K. (2003). Surface patterning via evaporation of ultrathin films containing nanoparticles. *J. Colloid and Interface Sci.*, 267(1):92–110.

[20] Zang, D., Tarafdar, S., Tarasevich, Y., Dutta Choudhury, M., and Dutta, T. (2019). Evaporation of a droplet: from physics to applications. *Phys. Rep.*, 804:1–56.